Role of Disorder in Thermal Transport A thesis proposal by

Jason M. Larkin

March 8, 2012

205 Scaife Hall

Department of Mechanical Engineering

Carnegie Mellon University

Thesis Committee

Associate Professor Alan McGaughey (Committee Chair), Mechanical Engineering

Professor Jonathan A. Malen, Mechanical Engineering

Professor Michael Widom, Physics

Professor Craig Maloney, Civil and Environmental Enginering

Contents

1 Motivation

1.1 Amorphous Systems

Understanding thermal transport in crystalline (ordered) systems requires detailed knowledge of phonons (Section 2.1), which are the quanta of energy associated with atomic vibrations in a periodic system.[2,14,54,63] By definition, phonons are non-localized vibrations which exist because of the translational order of the crystal. As an ordered system is disordered through the addition of defects, boundaries/interfaces, or amorphization, the vibrational modes which carry heat become localized and non-propagating and a new description is required. For completely disordered systems, such as amorphous materials, the thermal transport is modeled using completely localized vibrations (called *diffusons*) which propagate diffusively (as phonons do).[1] However, the propagation of these diffusons is (typically) much slower than the propagation of phonons which are able to carry heat over long distances before scattering. Thus, the thermal conductivity of the amorphous phase is typically several orders of magnitude less than the crystalline phase.[5,19] The first evidence of localized modes (diffusons), was reported by Keppens et al. using heat capacity, elastic constant and inelastic neutron-scattering measurements.[27] In general, the thermal transport in amorphous and disordered systems has contributions from localized vibrations and very-long wavelength phonon modes (see Section 3.6). Experimental measurements have shown a film thickness dependence of thermal conductivity in amorphous silicon[44] and hydrogenated amorphous silicon thin films,[32] which demonstrates the contribution of phonons to the thermal conductivity. Amorphous silicon/silica thin films are used in a variety of applications where managing thermal transport is important. Anomalously high measurements of thermal conductivity amorphous silicon thin films[66] suggest that the relative contributions of ordered (phonon) and disordered vibrations to the thermal conductivity in amorphous systems requires more understanding.[69]

1.2 Thermoelectric Energy Conversion using Large Unit Cell Skutterudites

Thermoelectric energy generation - the transformation of waste heat into useful electricity - is a promising source of sustainable energy.[15] Thermoelectric materials directly convert temperature differences into electric voltage, or *vice versa*, as a result of their intrinsic (atomic-level) electronic and thermal properties. Thus, thermoelectric materials can also be used in refrigeration applications. The performance of a thermoelectric device can be

quantified through the dimensionless thermoelectric figure of merit,

$$ZT = \frac{S^2 \sigma T}{k_{thermal}}, \tag{1}$$

where T is the average device temperature, S is the Seebeck coefficient (the ratio of the induced thermoelectric voltage to the applied temperature difference), σ is the electrical conductivity, and $k_{thermal}$ is the thermal conductivity. The thermal conductivity contains contributions from electrons and phonons (see Section 2.1). For thermoelectric devices to be competitive with traditional power generation cycles requires $ZT > 3$.[10] However, for waste heat retrieval any improvement in ZT is desirable. Achieving this performance is challenging because the electrical and thermal properties in ZT are coupled in the majority of materials.[10,15] The ideal thermoelectric can be thought of as an electron-crystal/phonon-glass (high σ, low $k_{thermal}$, see Fig. 1). Reducing $k_{thermal}$ has become a primary strategy in the design of new thermoelectric materials.[15] Using nanostructuring to reduce $k_{thermal}$ while maintaining good electrical properties has been identified as one possible strategy,[41] but such materials are costly. An emerging area of study in thermoelectric power generation is the use of large unit cell (LUC) crystals.[15,22] LUC crystals have an ordered (crystalline) structure,

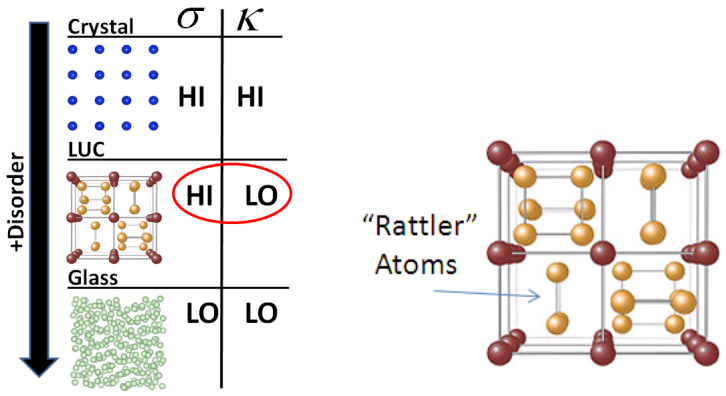

(a) (b)

Figure 1: (a) LUC Skutterudites can be thought of as "electron-crystals, phonon-glass". (b) sub-unit cell effects, including the role of "rattler atoms", must be considered when characterizing the thermal transport in these LUC materials.

but the basic building block (unit cell) of the crystal has a large number of distinct atoms (Fig. 1).[23,64,65] They are effectively disordered over length scales on the order of the atomic spacing and their thermal conductivities can be as low as a glass (amorphous material).[23,64,65] The key advantage of LUC materials is that they are still ordered from the standpoint of electrons, making them electron-crystal/phonon-glass materials. Current LUC crystals have

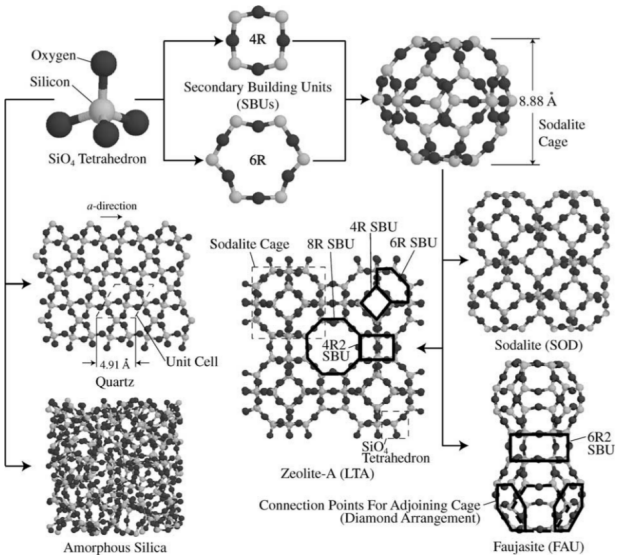

Figure 2: Silica structure building blocks and materials, incuding the LUC Zeolites. Diverse sub-unit cell structures are possible, which are likely to display unique localized vibrational properties that play an important role in thermal transport.

$ZT < 3$[23,64,65] and more research is required to improve their thermoelectric performance. The LUC crystals to be studied here are Skutterudite.[23] Experimental measurements of the thermoelectric properties of Skutterudites show intriguing potential,[23,64,65] but more research is required to achieve high ZT. Current research is focused to increasing ZT by reducing the $k_{thermal}$.[11,27,49] The mechanisms for thermal conductivity reduction in LUC materials are still being investigated.[47,49] Some work explains the reductions in thermal conductivity in terms of a phonon picture,[43,58,65] while other work suggests that sub-unit cell effects are most important.[12] It is thus difficult to develop an optimization strategy reducing the thermal transport in LUC Skutterudite materials without understanding the relative contributions of both phonons and disordered vibrational modes.

1.3 Large Unit Cell Zeolites for Gas Adsorption

Zeolites are another class of LUC materials which are sometimes referred to as porous crystals, themselves a diverse group of materials characterized by large unit cells and Angstrom sized pores and channels.[38] The size of the pores is on the same scale as the dimensions of atoms and molecules, leading to the use of porous crystals as molecular sieves, catalysts, and gas storage applications.[16] There also is interest in the design of porous crystals with very low thermal conductivities for applications as rigid insulators and to protect stored gases from ambient temperature fluctuations which requires understanding the thermal transport

properties. The thermal transport in zeolites and other cage-like structures is dictated by both phonons[38] and localized vibrations which arise due to sub-unit cell effects.[17,45] Thomas et al. used molecular simulation to show that water molecules in carbon nanotubes scatter phonons with specific vibrational frequencies related to the vibrational properites of the nanotubes and molecules.[57] The same effects are seen in molecular simulation predictions of thermal transport in carbon nanotubes on silica substrates.[46] It is likely that adsorbed molecules in Zeolites play a similar role in scattering vibrations, but it is unclear which vibrational modes (phonons or localized) are affected.[42] To design thermal properties, the mechanisms by which heat is transferred in these materials must be understood.

1.4 Hypothesis

Based on the research provided in the above sections, the following hypothesis will be investigated in this work:

- *Hypothesis: the thermal transport in amorphous and disordered materials can be accounted for using simple, computationally cheap models by considering the contribution from ordered (phonons) and disordered vibrations.*

- *Hypothesis: understanding thermal transport in diverse LUC materials such as Skutterudites and Zeolite allotropes requires analysis of ordered (phonons) and sub-unit cell (disordered) vibrations.*

- *Hypothesis: it is likely that the thermoelectric performance of large unit cell Skutterudites has yet to be fully realized until the ordered (phonons) and disordered contributions to minimizing thermal conductivity is understood.*

2 Background

2.1 Vibrational Thermal Conductivity

Thermal conductivity in a material arises from both electronic (k_e) and vibrational (k_{vib}) contributions.[2,53] The electronic contribution is important in metals and is well described by the WiedemannFranz law, increasing linearly with the electrical conductivity and temperature. For dielectric and semiconducting materials, the vibrational contribution is dominant and

$$k_{thermal} = k_e + k_{vib} \approx k_{vib}. \tag{2}$$

In this work, only dielectric and semiconducting materials are considered. The energy carriers of the vibrational conductivity are phonons, which are the quanta of energy associated with atomic vibrations.[2,14,54,63] The vibrational conductivity can be derived at the carrier (phonon) level by solving the Boltzmann transport equation under the relaxation time approximation.[54,68] For a crystal (ordered) system, the expression for the thermal conductivity is a sum over all phonon modes with mode specific properties,

$$k_{vib,\mathbf{n}} = \sum_{\boldsymbol{\kappa}} \sum_{\nu} c_{ph}(\boldsymbol{\kappa}_\nu)\, v^2_{g,\mathbf{n}}(\boldsymbol{\kappa}_\nu)\, \tau(\boldsymbol{\kappa}_\nu)\,. \tag{3}$$

Here, $\boldsymbol{\kappa}$ are the allowed wavevectors in the system (see Section A.3), ν is the phonon polarization with vibrational frequency $\omega(\boldsymbol{\kappa}_\nu)$, $c_{ph}(\boldsymbol{\kappa}_\nu)$ is the mode specific heat, $v^2_{g,\mathbf{n}}(\boldsymbol{\kappa}_\nu)$ is the phonon group velocity in the direction $\mathbf{n}$, and $\tau(\boldsymbol{\kappa}_\nu)$ is the phonon lifetime. The phonon lifetime can be recast as a mean free path by

$$\Lambda(\boldsymbol{\kappa}_\nu) = |v_{g,\mathbf{n}}|\tau(\boldsymbol{\kappa}_\nu)\,, \tag{4}$$

which is useful for describing the scattering of phonons over length scales that can be compared to relevant length scales in the system (see Section 3.2).

2.2 Range of Vibrational Thermal Conductivity

The vibrational conductivity of a variety of solids (single species crystals (e.g., Si, diamond), amorphous solids (e.g., amorphous silica and carbon), and Large Unit Cell (LUC) materials (e.g., Skutterudites, Zintl compounds)) are showin in Fig. 3. Over the range of solids and temperatures, the vibrational conductivity can vary by up to 10^6. The vibrational conductivity of LUC materials are comparable to those of the amorphous solids. The vibrational conductivity of amorphous solids is refered to as the "glass" or amorphous

limit (see Section 1.1), which usually represents the lower bound of vibrational conductivity for a system which has a crystalline phase.[5,6] The behavior of vibrational conductivity at low temperatures follows a scaling because phonons are bosons, which follow Bose-Einstein statistics.[19,54,56] Once a significant number of phonon modes become occupied (particularly at high frequency), the vibrational conductivity becomes dependent on the sample boundary size which limits the phonon mean free paths (see Section 3.2). This boundary scattering causes a maximum in the vibrational conductivity at some temperature, above which the vibrational conductivity decreases due to increasing phonon scattering (see Section 3.1). The range of decreasing vibrational conductivity with temperature can be estimated using the Debye temperature (T_D) which is calculated using the debye frequency (ω_D) of the system.[2,54] For amorphous and disordered materials, the vibrations in the system are not completely characterized by phonons. With the exception of very long wavelength modes, the vibrational modes are localized and do not propagate like phonons in a crystal (see Section 3.4). This is the reason that the vibrational conductivity of amorphous and LUC materials in Fig. 3 generally increase monotonically with temperature. For disordered materials, Eq. (3) can only describe the very low-frequency phonon-like modes which have a non-zero group velocity. However, Eq. (3) is still commonly used to estimate vibrational conductivity in an amorphous disordered system. Here, one typically assumes one of the following:

- The group velocity for all the modes is equal to the speed of sound and the mean free path is given by the average interatomic distance.[18,28] This is referred to as the Einstein model.

- The group velocity for all the modes is equal to the speed of sound and the lifetime (mean free path) is given by the inverse of the mode frequency (half the mode wavelength, see Section 4.1).[5] This is referred to as the Cahill-Pohl (CP) model.

This approach can be used to estimate a lower limit to the vibrational conductivity in amorphous and disordered systems.[5,6] However, theory,[1] experimental measurements,[21] and simulation results[51] show that this approach can give only a qualitative description of the vibrations which contribute to the thermal conductivity in disordered systems (see Section 3.4).

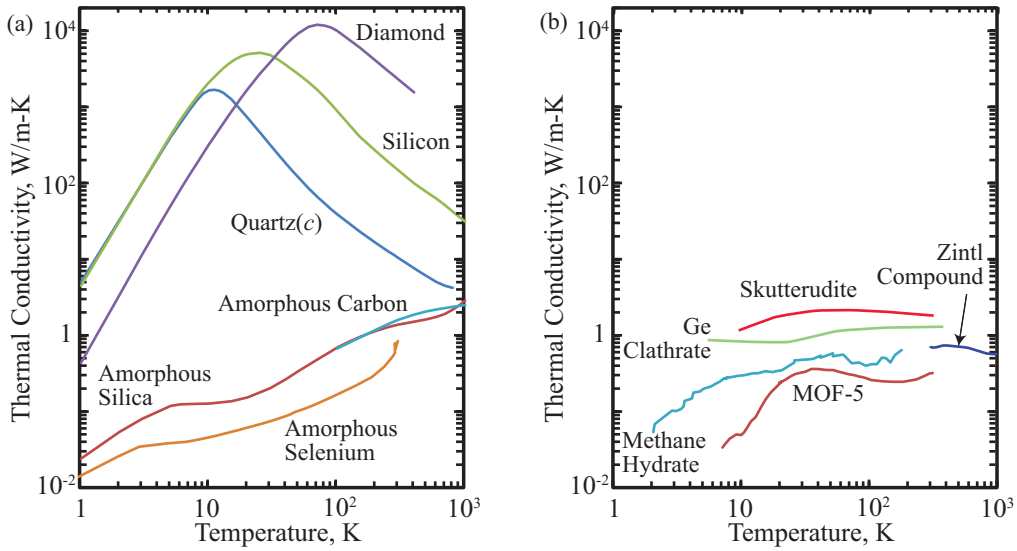

Figure 3: Temperature dependence of the vibrational conductivity of a variety of solids: (single species crystals (e.g., Si, diamond), amorphous solids (e.g., amorphous silica and carbon), and Large Unit Cell (LUC) materials (e.g., Skutterudites, Zintl compounds)). Over the range of solids and temperatures, the vibrational conductivity can vary by up to 10^6. The vibrational conductivity of LUC materials are comparable to those of the amorphous solids. The vibrational conductivity of amorphous solids is refereed to as the "glass" or amorphous limit, which usually represents the lower bound of vibrational conductivity for a system which has a crystalline phase.[5,6]

3 Preliminary Work

3.1 Vibrational Thermal Conductivity in Ordered Materials

For ordered (crystalline) systems, there are many phonon transport models which attempt to express Eq. (3) as an integral quantity,[9,25]

$$k_{vib} = \int_0^{\omega_{max}} c(\omega)_{ph} D(\omega) D_{ph}(\omega) d\omega, \tag{5}$$

whose terms are sometimes referred to as the properties of the frequency-dependent phonon spectrum. While Eq. (5) useful for examining general trends in vibrational conductivity, in a real system the phonon properties do not follow an analytical form (see . (3)). In a harmonic crystalline system, phonon lifetimes are infinite, making the k_{vib} infinite (see Appendix C). The scattering of phonons in a pure crystal arises from phonon-phonon interactions, which arise from the anharmonicity of the interatomic potentials. The strength of the anharmonicity dictates the strength of the phonon-phonon interactions and hence the lifetime reduction.[61] A simple model for the phonon-phonon scattering of acoustic mode phonons (dominant in crystalline thermal transport) is

$$\tau_{p-p} = \frac{(6\pi^2)^{1/3} \bar{m} v_g v_p^2}{2V^{1/3} \omega^2 \gamma^2 T}, \tag{6}$$

where $\bar{m}$ is the average crystal mass, v_g is the acoustic branch group velocity, v_p is the acoustic branch phase velocity, V is the system volume, ω is the phonon frequency, γ is the mode dependent Gruneisen parameter, and T is the temperature.[9,25] The form of Eq. (6) and its parameters are able to explain several general trends:

- It is phonon-phonon scattering which is responsible for the decrease of thermal conductivity with temperatures seen in Fig. 3.
- The reduced vibrational conductivity of germanium compared to silicon can be explained in both in terms of the $\bar{m}$ (germanium has a larger density ρ than silicon) and the group velocity (germanium has a smaller bulk modulus B, and $v_g \propto \sqrt{B/\rho}$.
- The decreased vibrational conductivity of systems which are highly anharmonic, such as weak covalently and Van der Waals bonded systems,[13] is accounted for by the Gruneisen parameter. For a purely harmonic system, the mode specific Gruneisen parameter is zero and the phonon lifetimes are infinite.

The temperature dependence of crystalline and amorphous thermal conductivity can be investigated using Molecular Dynamics (MD) simulation and the Green-Kubo method.[37]

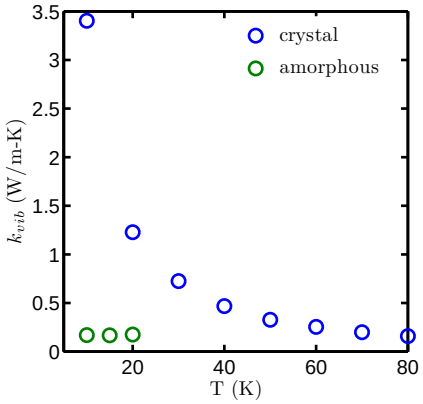

Figure 4: The temperature dependence of crystalline and amorphous Lennard-Jones samples predicted using MD simulations and the Green-Kubo method.[37] For the crystal the vibrational conductivity follows a $1/T$ scaling (consistent with the phonon-phonon lifetime scaling in Eq. (6)) , while the amorphous vibrational conductivity is temperature independent. Both of these trends are due to the lack quantum mechanical effects in the classical MD simulations.

These MD simulations are classical and do not include any quantum mechanical effects (Section 1.1). The Green-Kubo technique has been shown to accurately predict thermal transport for finite size systems.[37] Here, model Lennard-Jones (LJ) crystal and amorphous samples are used to predict the thermal conductivity as a function of temperature (see Fig. 4).[37] For the crystal the vibrational conductivity follows a $1/T$ scaling (consistent with the phonon-phonon lifetime scaling in Eq. (6)) , while the amorphous vibrational conductivity is temperature independent. Both of these trends are due to the lack quantum mechanical effects in the classical MD simulations. The phonon-phonon scattering model Eq. is typically used with the Debye approximation, which assumes linear and isotropic dispersion $\omega = v_g \kappa$ (or some variation[9,25]). If the dispersion is linear, the frequency dependent phonon density of states is

$$D(\omega) = A\omega^2, \tag{7}$$

where A is a constant related to the material properties.[2] In a real system, the phonon dispersion is not linear, which can be demonstrated by calculating the density of states for a LJ crystal (Fig. 5(a)). The density of states is calculated using Lattice Dynamics (LD) calculations.[14] At low frequencies the density of states follows a Debye type scaling (ω <15), but diverges at high frequency due non-linearity of the phonon dispersion (see Section 3.5). For the amorphous system, the majority of vibrations in the system are not phonons and thus the density of states only follows Debye scaling at very low frequencies (long wavelengths,

see Section 3.5). The phonon lifetimes in a LJ crystal also do not strictly follow the lifetime

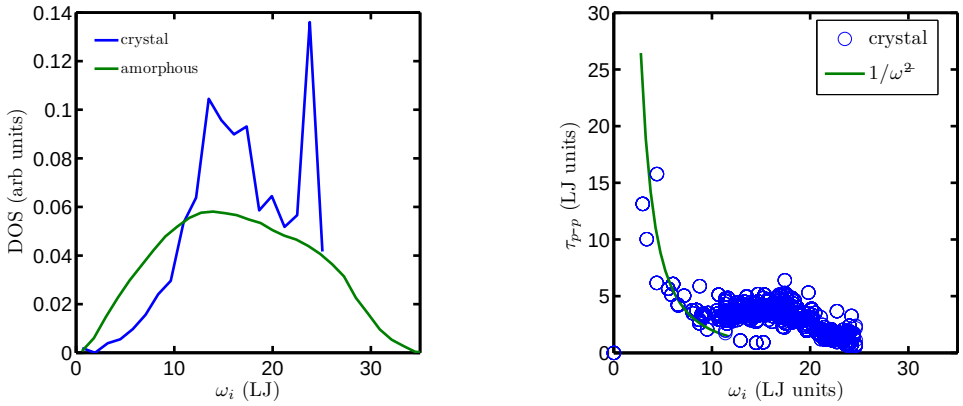

(a) (b)

Figure 5: (a) Density of states for a crystal and amorphous Lennard-Jones system (total number of atoms is 2048). For the crystal, the density of states roughly follows a Debye scaling at low frequencies (ω <15), above which the density of states does not follow an analytical form due to the non-linear dispersion. For the amorphous system, the majority of vibrations in the system are not phonons and thus the density of states only follows Debye scaling at very low frequencies. (b) Phonon lifetimes as a function of frequency at T=20 K for the same Lennard-Jones crystal used to calculate the density of states in Fig. 5(a). The lifetimes roughly follow the scaling with frequency in Eq. (6) over the same frequency interval as the Debye scaling in the density of states (ω <15).

scaling model in Eq. (6). The phonon lifetimes for the LJ crystal are predicted using the Normal Mode Decomposition (NMD) method (Appendix A.2) for a system size $N_0 = 8$ (2048 atoms) at T=20 K. For the LJ crystal, the phonon lifetimes scale with ω^{-2} over roughly the same frequency range as the Debye scaling of the density of states, see Fig. (5(b)). For the predicted vibrational conductivity of this system (k_{vib} = 1.2 W/m-K), only 45.6% of the contribution comes from phonons which roughly follow the Debye approximation (for ω <15). These considerations demonstrate the usefulness and limitations of analytical models used to replace Eq. (3).

3.2 Phonon Scattering Mechanisms

The various phonon scattering mechanisms described in this section scatter phonons with varying strength across the phonon spectrum. The phonon-phonon scattering described by Eq. (6) scatters phonons strongly across a wide frequency range. Phonon scattering by

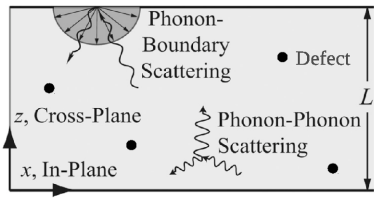

Figure 6: The various phonon scattering mechanisms scatter phonons with varying strength across the frequency spectrum. The phonon-phonon scattering is intrinsic and exists even in perfect crystals. Boundary scattering is responsible for decreasing the long lifetimes (mean free paths) of low frequency phonons which carry a significant amount of heat. Defect scattering is of Rayleigh type, where high frequency modes are scattered most strongly.

boundaries (τ_b) and defects (τ_b) affect very different intervals of the frequency-dependent phonon spectrum (Eq. (5)). A simple and effective model for boundary scattering is to assume diffuse scattering, which for the case of a thin film (Fig. 6) gives

$$\tau_b = L/v_g. \tag{8}$$

When the phonon mean free path is greater than the film thickness, it's mean free path is limited by this length scale. The concept can be extended to nanostructures of arbitrary geometry.[39] This boundary scattering model can account for several effects:

- It is boundary scattering which is dominant and responsible for slowing the rate of vibrational conductivity increase at low temperatures in Fig. 3.
- Boundary scattering describes the decrease in vibrational conductivity in thin films of decreasing thickness and other nanostructures of various decreasing system geometries.[39]

Boundary scattering is responsible for decreasing the long lifetimes (mean free paths) of low frequency phonons which carry a significant amount of heat, making it particularly effective at decreasing the thermal conductivity of systems with length scale of 100s of μm and less.[39] Defect scattering in the form of atomic mass and/or size variation can be modeled assuming the defects are a perturbation, by

$$\frac{1}{\tau_d} = \frac{V\omega^4}{4\pi v_p^2 v_g}\left(\sum_i c_i(1 - m_i/\bar{m})^2 + \sum_i c_i(1 - r_i/\bar{r})^2\right), \tag{9}$$

where c_i is the fraction, m_i is the mass, and r_i is the radius of species i and $\bar{r}$ is the average atomic radius.[29,30] The frequency dependence is the same as Rayleigh scattering, where high frequency modes are scattered most strongly.

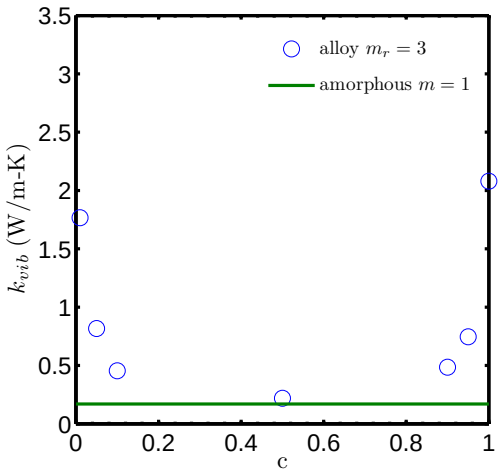

Figure 7: The vibrational conductivity of LJ alloys predicted using MD simulations and the Green-Kubo method. The predicted thermal conductivities are for a LJ alloy of the form $m^a_{1-c}m^b_c$, where $m^a = 1$, $m^b = 3$, and $m_r = m^a/m^b = 3$ (in LJ units). As the alloy concentration is increased perturbatively, the vibrational conductivity drops quickly and saturates to a minimum at $c = 0.5$. For $c = 0.5$ the system is heavily disordered and the vibrational conductivity approaches that of an amorphous system.

3.3 Dilute Alloys

Experimental measurements[7] and atomistic simulation predictions[52] show phonons still dominate the thermal transport in weakly perturbed systems such as dilute alloys.[9] The reduction in phonon lifetimes can be accounted for using Matthiessen's rule,

$$\frac{1}{\tau} = \frac{1}{\tau_{p-p}} + \frac{1}{\tau_b} + \frac{1}{\tau_d}, \tag{10}$$

where τ_{p-p} accounts for phonon-phonon scattering, τ_b accounts for boundary scattering, τ_d accounts for defect scattering. These scattering mechanisms can be understood by considering the phonon mean free path $\Lambda(\boldsymbol{\kappa}_\nu)$ and the illustration in Fig. 6. The vibrational conductivity of LJ alloys can be predicted using MD simulations and the Green-Kubo method (Fig. 7). The predicted thermal conductivities are for a LJ alloy of the form $m^a_{1-c}m^b_c$, where $m^a = 1$, $m^b = 3$, and $m_r = m^a/m^b = 3$ (in LJ units). As the alloy concentration is increased perturbatively, the vibrational conductivity drops quickly and saturates to a minimum at $c = 0.5$. For $c = 0.5$ the system is heavily disordered and the vibrational conductivity approaches that of an amorphous system.

3.4 High Concentration Alloys and Glasses

The models for phonon scattering mechanisms described in Section 3.2 are successful for dilute alloys ($c < 0.1$).[29,30] However, as the alloy concentration is increased, the vibrational modes become localized and non-propagating and a new description of the vibrational modes which carry the heat is required. For even more disordered systems, such as amorphous materials, the thermal transport is modeled using completely localized vibrations (called *diffusons*) which propagate diffusively, as phonons do.[1] However, the propagation of these diffusons is (typically) much slower than the propagation of phonons which are able to carry heat over long distances before scattering. Thus, the vibrational conductivity of amorphous phase is typically several orders of magnitude less than crystalline phase.[5,19] The diffuson theory of Allen and Feldman is different than the phenomenological models discussed in Section 1.1 in that the only allowed wavevector is strictly $\kappa = 0$ since the system is disordered. In reality, the vibrational conductivity has contributions from very-long wavelength phonon-like modes (see Section 3.2). The disordered contribution to vibrational conductivity, k_{AF}, is given by

$$k_{AF} = \sum_i C(\omega_i) D_{AF}(\omega_i) \tag{11}$$

where $C(\omega_i)$ and $D_{AF}(\omega_i)$ are the diffuson mode specific heat and diffusivity. The vibrational conductivity at low temperatures in disordered and amorphous materials is due to the low temperature behavior of the specific heat $C(\omega_i)$, which is dictated by Bose-Einstein statistics.[1] The theory of Allen and Feldman is purely harmonic. In the classical harmonic limit, $C(\omega_i) = k_B$ and k_{AF} is temperature independent, which can be used to understand the amorphous LJ temperature independence of vibrational conductivity in Section 3.1. Taking the phonon mode specific heat to be $c_{ph}(\boldsymbol{\kappa}_\nu) = k_B$, the phonon mode specific vibrational conductivity (Eq. (3)) can be written as

$$k_{vib,\mathbf{n}} = \sum_{\boldsymbol{\kappa}} \sum_{\nu} k_B D_{ph}(\boldsymbol{\kappa}_\nu)\,, \tag{12}$$

and the vibrational conductivity is determined by the phonon mode diffusitivies, defined as

$$D_{ph}(\boldsymbol{\kappa}_\nu) = v(\boldsymbol{\kappa}_\nu)^2\, \tau(\boldsymbol{\kappa}_\nu)\,. \tag{13}$$

This concept is useful for understanding how the relevant phonon properties (lifetime and group velocity) affect the thermal transport. It is also useful for comparing the relative transport strength of diffusons and phonons. Fig. 8 plots the phonon and diffuson mode diffusivities of a 256 atom LJ crystal and amorphous system at T = 20 K. The number of vibrational modes is the same for these two systems, but the relative magnitudes of the

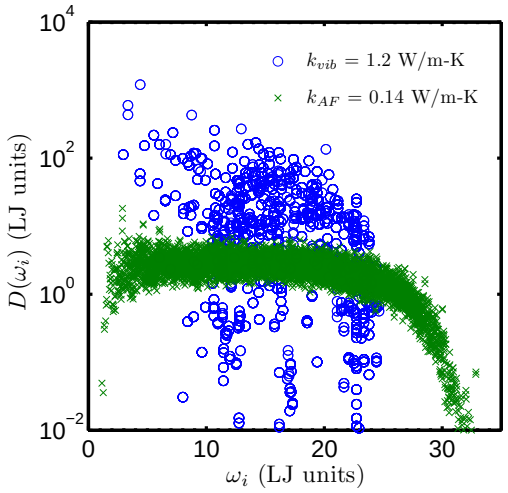

Figure 8: plot comparison of phonon diffusivity versus AF mode diffusivity for a 256 atom LJ crystal and amorphous system. For both systems, the total number of vibrational modes is the same.

diffusivities vary greatly. The phonons diffusivities are generally greater than the diffuson diffusivities. However, Brioullin zone boundary (see Section A.3) phonon modes have a finite lifetime but vanishing group velocities, giving $D_{ph}(\boldsymbol{\kappa}_\nu) = 0$.[14] For crystalline systems with many atoms in the unit cell, the presence of optical phonon modes begins to trap heat in low-group velocity branches ($D_{ph}(\boldsymbol{\kappa}_\nu) \approx 0$, see Section 3.5), making the distinction between phonons and diffusons diffuclt. Based on their contribution to vibrational conductivity, these low diffusivity optical phonons are thermally indistinguishable from diffusons. The parameters defining the phonon diffusivity (phonon lifetime and group velocity) are generally well-understood. In particular, design strategies to minimize both of these parameters exist (see Sections 3.2 and 3.5). However, the design strategies to control the diffusons diffusivities (D_{AF}) are not well understood.[1,51] The diffuson theory does not consider the effects of anharmonicity, which cane be investigated using a combination of MD simulations and LD calculations.[51]

3.5 Importance of Phonon Dispersion

Real phonon dispersion in crystalline systems is non-linear. For single mass species LJ crystal, the choice of unit cell is will dictate the allowed wavevectors (see Section A.3) and hence the phonon dispersion. Dispersion plots for the primitive ($b = 1$) and cubic conventional ($b = 4$) LJ FCC unit cells for wavevectors in the $2\pi/a[100]$ direction are shown in Fig. 9 (a) and (b). For the primitive and cubic conventional unit cells, the Brioullin zone bound-

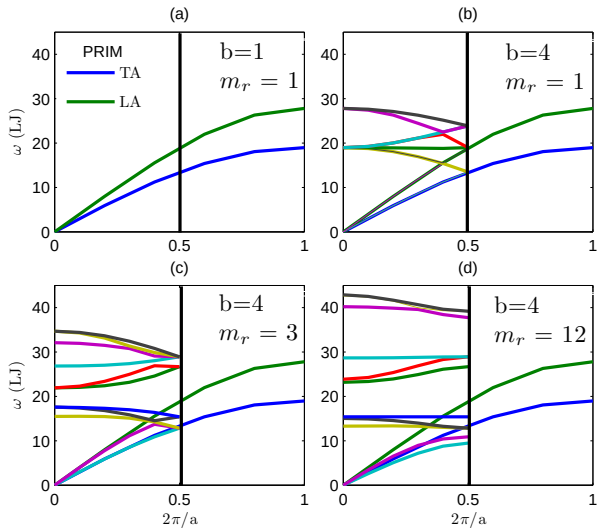

Figure 9: Dispersion plots for Lennard-Jones systems with varying number of atoms in the unit cell ($b = 1..4$) and mass ratio (m_r) for wavevectors in the direction $2\pi/a[100]$. (a) Dispersion plot using the FCC primitive unit cell ($b = 1$), which shows that only acoustic phonon branches exist in the system. The edge of the Brillouin zone in this direction is $2\pi/a[100]$. (b) Dispersion plot using the cubic conventional unit cell ($b = 4$), where every atom in the unit cell is identical ($m_r = 1$). Compared to the primitive cell, the Brillouin zone edge is at $\pi/a[100]$ where the acoustic branches have been "folded in".[59] Other than these considerations, the choice of unit cell for the single species system does not affect the dispersion. (c) System with two unique atom types in the conventional unit cell with a mass ratio $m_r = 3$, which creates optical branches with low group velocity and reduced group velocity acoustic branches. (d) System with $b = 4$ unique atoms types in the unit cell with high mass ratio ($m_r = 12$), which increases the number of optical branches and further reduces the acoustic group velocities.

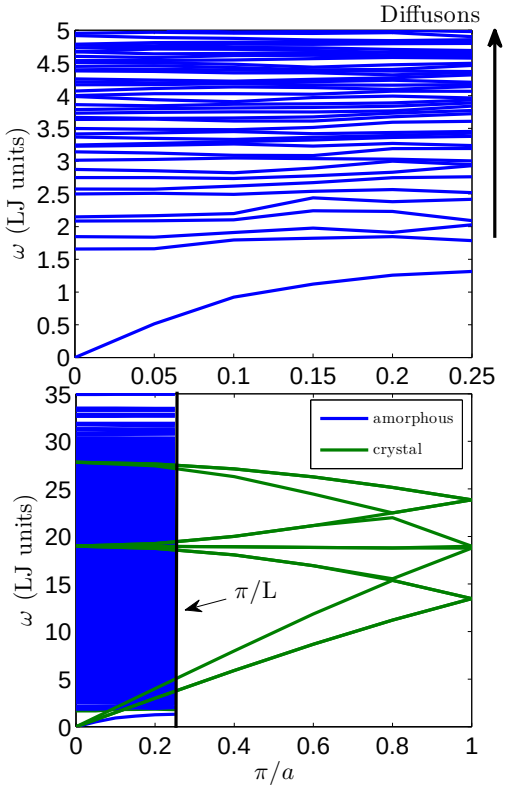

Figure 10: Dispersion of a 256 atom amorphous Lennard-Jones solid with simulation cell size $L = 4a$, where a is the FCC crystal lattice constant of the LJ system. The phonon-like acoustic group velocity (sound speed) can be detected at small but finite wavevector. The vast majority of modes in the system are localized vibrations (diffusons) which appear as optical branches with nearly zero group velocity.

ary in this direction is defined by $2\pi/a$ and π/a. For Fig. 9 (c) and (d), the conventional cubic unit cell contains two (c) and four (d) unique atoms with varying mass, the largest mass ratio labeled as m_r. Increasing the mass ratio m_r of the species in the unit cell increases the gap between optical and acoustic branches and decreases the acoustic group velocities. The Debye model (assumption of linear dispersion) largely overestimates the vibrational conductivity of high mass ratio (e.g. BaO) unit cells because of these reductions in group velocity.[58] The effect of group velocity reduction is particularly effective in reducing vibrational conductivity because the phonon diffusivities are proportional to v_g^2 (see Section 3.5). Phonon dispersion in multi-atom unit cell crystals contains optical phonon branches, which have low group velocity and thus contribute little to vibrational conductivity (see Section 3.5). More optical branches can be introduced by "zone-folding", caused by increasing the number of atoms in the unit cell (Fig. 9). Zone-folding traps heat in $b-1$ optical branches and decreases the acoustic mode group velocities.[55] For an amorphous material (see Section 3.5), this folding trend is continued until nearly all of the vibrational modes in the system are trapped in optical branches with virtually zero group velocity (Fig. 10). In the amorphous limit ($b = \infty$), the zone-folding effect would suggest that the heat is transported solely in optical modes as the acoustic phonon contribution goes to zero. In reality, thermal transport in amorphous materials has contributions from phonons and localized vibrations (see Section 1.1). The presence of acoustic phonon-like modes in amorphous materials can be demonstrated by considering an amorphous system of finite size. Fig. 10 shows the dispersion of a 256 atom amorphous Lennard-Jones solid with simulation cell size $L = 4a$, where a is the FCC crystal lattice constant of the LJ system. Since periodic boundary conditions are used, the simulation cell is the unit cell with lattice constant $L = 4a$. In this sense the amorphous LJ sample is a large unit cell material. By considering small but finite wavevectors in the direction $\pi/L[100]$, the sound speed (acoustic group velocity) can be detected by the presence of a single acoustic type branch (vanishing frequency at $\kappa = [000]$). The rest of the vibrational modes in the system are trapped in optical modes with virtually zero group velocity. The lowest finite frequency modes at $\kappa = [000]$ are the phonon like modes which can be supported within the amorphous large unit cell.[1,62] The rest of the finite frequency modes at $\kappa = [000]$ are the diffusons, which are non-propagating localized vibrations (see Section 3.4).

3.6 Phonons in Amorphous Materials

The diffuson theory is different than the phenomenological models discussed in Section 1.1 in that the only allowed wavevector is strictly $\kappa = 0$ since the system is disordered. In

reality, the vibrational conductivity has contributions from very-long wavelength phonon-like modes. Accordingly, the total vibrational conductivity in a disordered or amorphous system is the sum of contributions from diffusons and phonons,

$$k_{vib} = k_{AF} + k_{ph}. \tag{14}$$

Using the Green-Kubo method (see Section 3.1), the total vibrational conductivity of amorphous Lennard-Jones argon has been predicted to be $k_l = 0.17$ W/m-K. The diffuson contribution is predicted to be $k_{AF} = 0.14$ W/m-K, which suggests $k_{ph} = 0.03$ W/m-K. Similar atomistic predictions have been made for amorphous silicon, where the phonon contribution was shown to be $k_{ph} = 0.5k_{vib}$.[24] However, the definition of the allowed wavevectors, and hence the phonon properties of the amorphous system, is not well understood.[24]

4 Proposed Work

The preliminary research and work discussed in Sections 1, 2, and 3 will inform the proposed work discussed in the following sections. In particular, the hypothesis presented in Section 1 will motivate the outcomes of this work.

4.1 Quantify Thermal Transport in Amorphous and Disordered Materials

Hypothesis: the thermal transport in amorphous and disordered materials can be accounted for using simple, computationally cheap models by considering the contribution from ordered (phonons) and disordered vibrations. Thermal transport in crystals, alloys, and amorphous samples using model LJ systems will be studied to quantify and characterize the ordered and disordered contributions to lattice thermal conductivity. In particular, a more rigorous way to classify vibrational modes in disordered alloys and amorphous samples as phonon-like or diffuson will be investigated. These results will be compared to the phenomenological Einstein and Cahill-Pohl models,[5,18,28] which assume phonon-like properties for the disordered vibrational modes. In the Cahill-Pohl model,[8] the group velocity of all the vibrational modes is assumed to be the sound speed,

$$v_g = v_s \propto \sqrt{B_{glass}/\rho}, \tag{15}$$

and the phonon mean free paths scale with the wavelength of the mode,

$$\Lambda_{glass} = \lambda/2. \tag{16}$$

It is unclear what meaning a wavelength has for of the diffuson vibrational modes. Given experimental measurements[32,44,66,69] and atomistic predictions,[24,51] it is more likely that the phonon-like modes in disordered materials follow simple Debye-type scalings of their properties (Sections 3.1 and 3.5). This presents the opportunity of modeling thermal transport in disordered and amorphous materials using simple scaling models and diffuson theory, both of which are computationally inexpensive compared to more complicated thermal transport models.[61] It is also unclear how to properly define the allowed wavevectors in an amorphous or disordered system (see Appendix A.3). Because of this, the way phonons interact with diffusons in these systems is not understood and will be investigated. Selection rules which determine allowed phonon-phonon interactions are based on two conservation rules. First, conservation of crystal momentum dictates that the wavevectors of the phonons involved in a 3-phonon process satisfy

$$\boldsymbol{\kappa} + \boldsymbol{\kappa}'' = \boldsymbol{\kappa}'' + \boldsymbol{G} \tag{17}$$

where $\boldsymbol{G}$ is a reciprocal lattice vector.[14,63] Second, the frequencies (energies) of the phonons invovled in the scattering process satisfy[14,63]

$$.\omega(\boldsymbol{\kappa}_{\nu}) + \omega(\boldsymbol{\kappa}'_{\nu'}) = \omega(\boldsymbol{\kappa}''_{\nu''}) \tag{18}$$

Given these conservation rules, it is unclear how the phonons which exist in amorphous and disordered materials interact with other phonons and disordered diffuson modes. The Allen Feldman diffuson theory is a purely harmonic one, while the MD simulations performed in this work include the full anharmonicity of the LJ interatomic potential. The effect of anharmonicity will be investigated to determine what contribution it makes to thermal transport in disordered systems using LD calculations and MD simulations. Using the information gathered from the LJ calculations, *ab initio* (from first-principles)[3] calculations will be designed for real amorphous systems, such as amorphous silicon. *Ab initio* are computationally-intensive, but have high accuracy and predictive capability.[3]

4.1.1 Outcomes

The outcomes of this work will be:

- to develop methodology to identify relative contribution to thermal transport from phonons and diffusons in disordered LJ systems.
- to investigate the role of anharmonicity to thermal transport in disordered systems, which can determine if computationally cheap methods and models can make accurate predictions.
- to design and perform *ab initio* calculations to predict the thermal properties of real disordered systems such as amorphous silicon.

4.2 Investigate Thermal Transport in LUC Zeolites and Skutterudites

Hypothesis: understanding thermal transport in diverse LUC materials such as Skutterudites and Zeolite allotropes requires analysis of ordered (phonons) and sub-unit cell (disordered) vibrations, which are likely to be localized. The thermal transport in Zeolites and other cage-like structures is dictated by both phonons[38] and localized vibrations which arise due to sub-unit cell effects.[17,45] Diverse sub-unit cell structures are possible, which are likely to display unique localized vibrational properties that play an important role in thermal transport. For gas adsorption applications, the role of scattering is not understood. Thomas et al.

used molecular simulation to show that water molecules in carbon nanotubes scatter phonons with specific vibrational frequencies related to the vibrational properties of the nanotubes and molecules.[57] The same effects are seen in molecular simulation predictions of thermal transport in carbon nanotubes on silica substrates.[46] It is likely that adsorbed molecules in Zeolites play a similar role in scattering vibrations, but it is unclear which vibrational modes (phonons or localized) are affected.[42] Thermal transport in Zeolite structures will be investigated using LD calculations and classical MD simulations. Classical interatomic potentials exist which can describe the various Zeolite allotropes.[38] Sub-unit cell effects of thermal transport will be investigated in the these diverse structures where unique bonding environments and cage-like structures likely play an important role. *Hypothesis: it is likely that the thermoelectric performance of large unit cell Skutterudites has yet to be fully realized and requires understanding the ordered (phonons) and disordered contributions to the thermal transport to minimize thermal conductivity.* For many LUC materials, such as Skutterudites, two scalings of the vibrational conductivity (labled in Fig. 11 as κ_L) are shown for experimental measurements.[58] The vibrational thermal conductivity can be predicted using the Debye model (labled in Fig. 11 as κ_U), which predicts two scalings of κ_L with number of atoms in the unit cell b. The two scalings, $b^{-1/3}, b^{-1}$ are based on phonon-phonon or boundary dominant scattering.[58] The disagreement between the Debye model predictions and experimental measurements suggest the importance of the non-linear (non-Debye) dispersion (see Section 3.5) and sub-unit cell effects in determining the minimized vibrational conductivity in LUC materials. Much of the excitement surrounding Skutterudites has been focused on the prediction and observation of a phenomena termed "rattling", observed when the guest atom is under-constrained and weakly bound (see Fig. 1).[11,27,49] Experimentally, materials in which guest atoms are strong rattlers are found to exhibit extremely low k_{vib}.[47,49] While it is widely accepted that rattling atoms result in strongly localized modes, the mechanism by which rattler modes reduce k_{vib} is under debate. The reduction in k_{vib} has been attributed to resonant scattering by the guest atom.[12] However, the impact of rattling on the group velocity has recently been recognized as an alternative explanation of the low experimental k_{vib} (see Section 3.5).[43,65] Thermal transport in LUC Skutterudites will be investigated using a combination of LD calculations MD simulations. Several classical interatomic potentials exist which can be used to study general trends.[4,67] Ultimately, *ab initio* calculations will be designed for real Skutterudite systems.

4.2.1 Outcomes

The outcomes of this work will be:

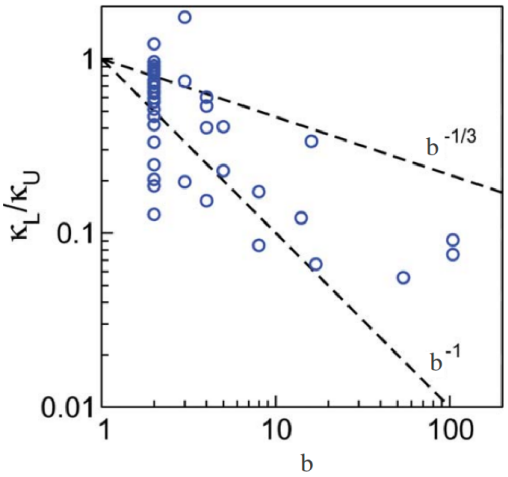

Figure 11: For many LUC materials, such as Skutterudites, two scalings of the vibrational conductivity (labled κ_L) are shown for experimental measurements.[58] The vibrational thermal conductivity can be predicted using the Debye model (labled as κ_U), which predicts two scalings of κ_L with number of atoms in the unit cell b. The two scalings, $b^{-1/3}, b^{-1}$, are based on phonon-phonon or boundary dominant scattering.[58] The disagreement between the Debye model predictions and experimental measurements suggest the importance of the non-linear (non-Debye) dispersion (see Section 3.5) and sub-unit cell effects in determining the minimized vibrational conductivity in LUC materials.

- to characterize sub-unit cell effects such as gas adsorption in Zeolites and rattling modes in Skutterudites.
- to identify design strategies to manage thermal conductivity in Zeolites and reduce the thermal conductivity in Skutterudites for thermoelectric conversion applications.

5 Outcomes and schedule

The schedule for my proposed research is:

Task	Fall 2011
Characterization of Disordered LJ Models	———
Investigate (an)Harmonic Contributions	
Task	**Summer 2012**
Investigate Transport in Amorphous Si using Ab-Initio Calculations	———
Investigate Transport in LUC using Classical Models	
Task	**Spring 2013**
Investigate Transport in LUC using Ab-Initio Calculations	———
Deliver thesis	

6 Biographical Sketch

Jason Larkin was born in Monroeville, PA. He obtained his Bachelor's of Science degree in mechanical engineering from the University of Pittsburgh in Spring 2007. He obtained his Master's of Science degree in mechanical engineering in summer 2009 with a thesis: Statistics of Particle Concentrations in Free-Surface Turbulence. He entered Carnegie Mellon in Fall 2009 where he is pursuing his PhD in mechanical engineering.

Awards

Northrop-Grumann Fellow, CIT Institute for Complex Engineered Systems (ICES) 2011 NSF Research Grant, University of Pittsburgh Department of Physics 2007-2009 2011 Bennett Presentation (Award for Best Presentation). October 2011 Cover article for Physics of Fluids.

Peer-reviewed Journal Publications

- J. M. Larkin J. E. Turney, A. D. Massicotte, C. H. Amon, A. J. H. McGaughey, "Comparison and Evaluation of Spectral Energy Methods for Predicting Phonon Properties", submitted Physical Review B.
- S. Stefanus, J. Larkin, W. Goldburg, A Search for Conformal Invariance in Compressible Two Dimensional Turbulence, Physics of Fluids 23 (2011) 105101. Selected for cover.
- J. Larkin, W. Goldburg, M.M. Bandi, Time-Evolution of a fractal distribution: Particle concentrations in free-surface turbulence, Physica D 239 14 (2010) 1264-1268.
- J. Larkin, W. Goldburg, Decorrelating a Compressible Turbulent Flow: an Experiment, Physical Review E 82, 016301 (2010).
- J. Larkin, M.M. Bandi, A. Pumir, W. Goldburg , Power-law distributions of particle concentration in free-surface flows, Physical Review E 80, 066301 (2009).

Conference Presentations

1. Predicting Phonon Properties of Silicon from First -Principles Calculations, J.M. Larkin, A.J.H. McGaughey, W.A. Al-Saidi, to be presented at 2012 ASME Summer Heat Trans-

fer Conference Puerto Rico, USA.

2. Comparison of Spectral Energy Methods for Predicting Phonon Properties, J.M. Larkin, A.D. Massicotte, J.E. Turney, C.H. Amon, A.J.H. McGaughey, to be presented at 2012 ASME Micro/Nanoscale Heat & Mass Transfer International Conference Atlanta, GA.

3. Predicting Thermal Conductivity of Defected Systems using the Spectral Energy Density, J.M. Larkin, A.D. Massicotte, J.E. Turney, C.H. Amon, A.J.H. McGaughey, 2011 MRS Fall Meeting Boston, MA.

4. Predicting Thermal Conductivity of Defected Systems using the Spectral Energy Density, J. Larkin 2011 Bennett Presentation (Award for Best Presentation).

5. Decorrelating a Compressible Turbulent Flow: An Experiment, J. Larkin, W. Goldburg (speaker), 2010 American Physical Society March Meeting Portland, OR.

6. Statistics of Preferential Particle Concentration in Free -Surface Turbulence, J. Larkin (speaker), M.M. Bandi, W. Goldburg, 2009 American Physical Society March Meeting Pittsburgh, PA.

7. Experimental Determination of the von Karman Constant in Turbulent Two Dimensional Soap Film Flows, Nicholas Guttenberg (speaker), Nigel Goldenfeld, Jason Larkin, Alisia Prescott, Hamid Kellay, Walter Goldburg, 2008 Meeting of the APS Division of Fluid Dynamics San Antonio, TX.

8. Turbulent Dynamics of a Hydraulic Jump in two dimensions: Soap Film Flow Jason Larkin (speaker), Walter Goldburg, Tuan Tran, Pinaki Chakraborty, Gustavo Goia, 2008 Meeting of the APS Division of Fluid Dynamics San Antonio, TX.

9. The Generalized Fractal Dimensions of a 2 -D Compressible Turbulence, J. Larkin (speaker), M.M. Bandi, W. Goldburg, 2008 American Physical Soci ety March Meeting New Orleans, LA.

10. Design of a Flow Chamber to Explore the Initiation and Development of Cerebral Aneurysms, Jason Larkin, John P. Barrow, A. M. Robertson 2007 Biomedical Engineering Society Meeting Undergraduate Presentation Los Angeles, CA

A Predicting Phonon Properties

A.1 Vibrations in Ordered Solids

In a crystal (periodic) system, the vibrations of atoms are described by a basis of eigenfunctions called phonon normal modes, which are determined by the properties of the crystal (see Appendix A.3). The eigenvalues of this basis are the phonon mode frequencies (energies).[14,63] The atomic velocities can be represented by the velocity normal mode coordinate, defined as[14]

$$\dot{u}_\alpha(\tbinom{l}{b};t) = \sum_{\boldsymbol{\kappa}',\nu}^{N,3n} \frac{1}{\sqrt{m_b N}} \exp\Big[i\boldsymbol{\kappa}' \cdot \mathbf{r}_0(\tbinom{l}{0})\Big] e^*(\tbinom{\boldsymbol{\kappa}}{\nu}\ \tbinom{b}{\alpha})\, \dot{q}(\tbinom{\boldsymbol{\kappa}}{\nu};t)\,. \tag{19}$$

Here, $\dot{q}(\tbinom{\boldsymbol{\kappa}}{\nu};t)$ represents the kinetic energy $T(\tbinom{\boldsymbol{\kappa}}{\nu};t)$ of the mode with phonon frequency $\omega_0(\tbinom{\boldsymbol{\kappa}}{\nu})$ by[14]

$$T(\tbinom{\boldsymbol{\kappa}}{\nu};t) = \frac{\dot{q}^*(\tbinom{\boldsymbol{\kappa}}{\nu};t)\,\dot{q}(\tbinom{\boldsymbol{\kappa}}{\nu};t)}{2}. \tag{20}$$

The phonon mode kinetic energies $T(\tbinom{\boldsymbol{\kappa}}{\nu};t)$ are used to calculate the phonon spectral energy denisty in Appendix A.2.

A.2 Predicting Phonon Lifetimes using Spectral Energy Denisty

The phonon normal mode coordinate is,

$$\dot{q}(\tbinom{\boldsymbol{\kappa}}{\nu};t) = \sum_{\alpha,b,l}^{3,n,N} \sqrt{\frac{m_b}{N}} \dot{u}_\alpha(\tbinom{l}{b};t)\, e^*(\tbinom{\boldsymbol{\kappa}}{\nu}\ \tbinom{b}{\alpha}) \exp[i\boldsymbol{\kappa}\cdot\mathbf{r}_0(\tbinom{l}{0})], \tag{21}$$

which form the basis for vibrations in ordered materials and represents the phonon mode kinetic energy. The normal mode kinetic energy can be transformed from the time domain t to the frequency domain ω by Parseval's theorem,[48]

$$T(\tbinom{\boldsymbol{\kappa}}{\nu};\omega) = \lim_{\tau_0\to\infty} \frac{1}{2\tau_0} \left| \frac{1}{\sqrt{2\pi}} \int_0^{\tau_0} \dot{q}(\tbinom{\boldsymbol{\kappa}}{\nu};t) \exp(-i\omega t) dt \right|^2. \tag{22}$$

Here, $T(\tbinom{\boldsymbol{\kappa}}{\nu};\omega)$ represents the spectral energy of the phonon normal mode with frequency $\omega(\tbinom{\boldsymbol{\kappa}}{\nu};\omega)$. Following the derivation in Appendix C, one arrives at the expression for the SED of a single phonon mode,

$$T(\tbinom{\boldsymbol{\kappa}}{\nu};\omega) = \frac{C_0(\tbinom{\boldsymbol{\kappa}}{\nu})}{2} \frac{\Gamma(\tbinom{\boldsymbol{\kappa}}{\nu})/\pi}{[\omega_0(\tbinom{\boldsymbol{\kappa}}{\nu}) - \omega]^2 + \Gamma^2(\tbinom{\boldsymbol{\kappa}}{\nu})}, \tag{23}$$

which is a Lorentzian function with center at $\omega_0(\binom{\boldsymbol{\kappa}}{\nu})$ and a half-width at half-maximum (linewidth) of $\Gamma(\binom{\boldsymbol{\kappa}}{\nu})$ and $C_0(\binom{\boldsymbol{\kappa}}{\nu})$ is a constant. We know from anharmonic lattice dynamics theory that the phonon linewidth is related to the phonon lifetime, $\tau(\binom{\boldsymbol{\kappa}}{\nu})$, by[31,34]

$$\tau(\tbinom{\boldsymbol{\kappa}}{\nu}) = \frac{1}{2\Gamma(\tbinom{\boldsymbol{\kappa}}{\nu})}. \tag{24}$$

The MD simulations we perform here are classical. For a classical system in the harmonic limit (i.e., temperature approaching zero) there is an equipartition of energy and $\sum_{\nu}^{3n} T(\binom{\boldsymbol{\kappa}}{\nu};\omega) = \sum_{\nu}^{3n} V(\binom{\boldsymbol{\kappa}}{\nu};\omega)$.[40] In an anharmonic system (i.e., a MD simulation), the assumption of equipartition of energy can be tested by predicting the system-level specific heat. By assuming equipartition of energy, the phonon SED at a particular wavevector is

$$\Phi(\boldsymbol{\kappa},\omega) = 2\sum_{\nu}^{3n} T(\tbinom{\boldsymbol{\kappa}}{\nu};\omega) = \sum_{\nu}^{3n} C_0(\tbinom{\boldsymbol{\kappa}}{\nu}) \frac{\Gamma(\binom{\boldsymbol{\kappa}}{\nu})/\pi}{[\omega_0(\binom{\boldsymbol{\kappa}}{\nu}) - \omega]^2 + \Gamma^2(\binom{\boldsymbol{\kappa}}{\nu})}, \tag{25}$$

which is a superposition of $3n$ Lorentzian functions with centers at $\omega_0(\binom{\boldsymbol{\kappa}}{\nu})$ (one for each polarization). For simplicity, we refer to $\Phi(\boldsymbol{\kappa},\omega)$ as Φ. Given a set of atomic velocities, Φ can be calculated using Eq. (33) and (42), and then fit using Eq. (45) to extract the phonon properties $\omega_0(\binom{\boldsymbol{\kappa}}{\nu})$ and $\tau(\binom{\boldsymbol{\kappa}}{\nu})$.

A.3 Allowed Wavevectors in Ordered Systems

The phonon spectral energy is defined for the allowed wavevectors of a crystal, which can be specified from the crystal structure's Bravais lattice and its basis, i.e. unit cell. A D-dimensional Bravais lattice is a collection of points with positions

$$\mathbf{u}_0(\tbinom{l}{0}) = \sum_{\alpha}^{D} N_\alpha \mathbf{a}_\alpha \tag{26}$$

where N_α and the summations if over the lattice vectors, $\mathbf{a}_\alpha$.[2] The basis (or unit cell) is the building block of the crystal and they are arranged on the points defined by the Bravais lattice. The equillibrium position of any atom in the crystal can be described by

$$\mathbf{u}_0(\tbinom{l}{b}) = \mathbf{u}_0(\tbinom{l}{0}) + \mathbf{u}_0(\tbinom{0}{b}) \tag{27}$$

where $\mathbf{u}_0(\binom{l}{0})$ is the equilibrium position of the l^{th} unit cell and $\mathbf{u}_0(\binom{0}{b})$ is the equilibrium position of the and b^{th} atom in the unit cell relative to $\mathbf{u}_0(\binom{l}{0})$. For the LJ systems studied here, the cubic conventional cells are used with four atoms per unit cell.[2] For our MD simulations, cubic simulation domains with periodic boundary conditions are used with $N_1 = N_2 = N_3 = N_0$.[37,60] The allowed wavevectors for such crystal structures are

$$\boldsymbol{\kappa} = \sum_{\alpha} \mathbf{b}_\alpha \frac{n_\alpha}{N_\alpha}, \tag{28}$$

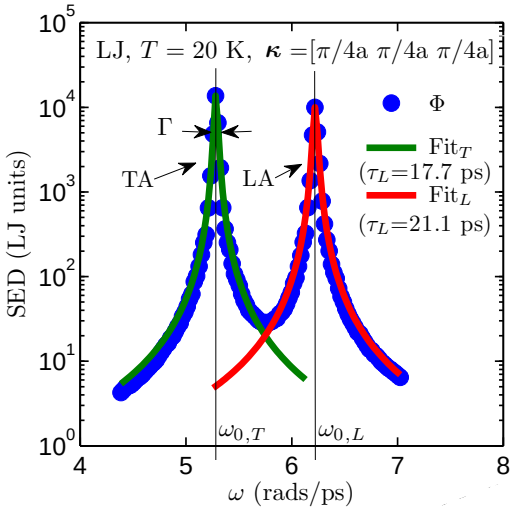

Figure 12: The SED (Φ) for the first three polarizations at the wavevector $[\pi/4a, \pi/4a, \pi/4a]$ for LJ argon at a temperature of 20 K. There are two degenerate transverse acoustic polarizations and one longitudinal acoustic polarization (of higher frequency).[14] When fitting the SED, the different polarizations can be fit individually using single Lorentzian peaks or as a superposition of peaks. Here the two peaks are fit individually with Φ plotted as a superposition. The predicted lifetimes of these polarizations, which are inversely proportional to the peak widths Γ, are provided in the legend.

where $\mathbf{b}_\alpha$ are the reciprocal lattice vectors[2] and $-N_\alpha/2 < n_\alpha \leq N_\alpha/2$, where n_α are integers and N_α are even integers.[60] The wavevectors are taken to be in the first Brioullin zone.[2]

A.4 Predicting Spectral Energy Density from Molecular Dynamics Simulations

Once the allowed wavevectors are specified (see Section A.3), the atomic velocities from an MD simulation can be used to calculate Φ. To calculate Φ, Eq. (42) requires the phonon mode eigenvector, which can be obtained *a priori* using quasi-harmonic lattice dynamics calculations using the finite temperature lattice constant.[35] The phonon frequencies and lifetimes are found by fitting Φ with Lorentzian functions using a non-linear least squares method. Both of these phonon properties are independent of the Lorentzian peak magnitude. The different polarizations can be fit individually using single Lorentzian peaks or as a superposition of peaks. At the temperatures studied in this work, we find that fitting single or simultaneous peaks results in less than five percent difference in the predicted lifetimes. The error from fitting the Lorentzian functions is between $5-10\%$ in the predicted lifetimes, with the error increasing with increasing temperature.*To illustrate the procedure, Φ was calculated using Eq. (42) for LJ argon with $N_0 = 8$ (2048 atoms) and $T = 20$ K. Φ for the three modes of lowest frequency and wavevector $[\pi/4a, \pi/4a, \pi/4a]$ is shown in Fig. 12. The lower frequency peak corresponds to the 2 degenerate transverse acoustic modes, while the higher frequency peak corresponds to the longitudinal acoustic mode.[14]

A.5 Thermal Conductivity

Once the frequencies and lifetimes of all phonon modes in the Brillouin zone are obtained, the bulk thermal conductivity in direction $\mathbf{n}$, $k_\mathbf{n}$, can be calculated from[68]

$$k_\mathbf{n} = \sum_{\boldsymbol{\kappa}} \sum_{\nu} c_{ph}(\overset{\boldsymbol{\kappa}}{\nu})\, v^2_{g,\mathbf{n}}(\overset{\boldsymbol{\kappa}}{\nu})\, \tau(\overset{\boldsymbol{\kappa}}{\nu})\,. \tag{29}$$

Here, c_{ph} is the phonon volumetric specific heat and $v_{g,\mathbf{n}}$ is the component of the group velocity vector in direction $\mathbf{n}$. Since the systems we consider are classical and obey Maxwell-Boltzmann statistics,[40] the specific heat is k_B/V per mode in the harmonic limit where V is the system volume. This approximation is used here and has been shown to be suitable for LJ argon[36] and SW silicon.[20] The group velocity vector is the gradient of the dispersion curves (i.e., $\partial\omega/\partial\boldsymbol{\kappa}$), which can be calculated from the frequencies and wavevectors using finite differences. In this work, the group velocities are calculated using finite difference and quasi-harmonic lattice dynamics because a very small finite difference can be used which

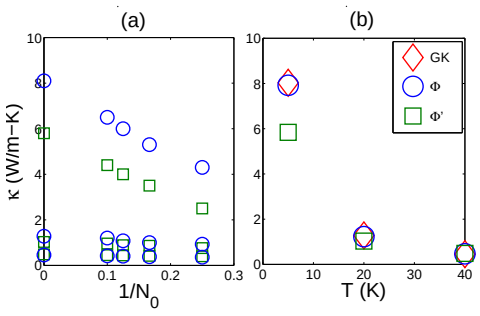

Figure 13: Thermal conductivity predictions for LJ argon calculated using phonon lifetimes predicted by Φ and Φ'.[26] (a) The finite simulation-size scaling extrapolation[24,60] is used to compare the results to bulk predictions made using the Green-Kubo method. (b) The bulk results for Φ and Green-Kubo are in good agreement temperatures of 20 and 40 K with those of other atomistic simulation methods.[60]

reduces the error.[35] To predict a bulk thermal conductivity, it is necessary to perform a finite simulation size scaling procedure as discussed in Appendix B.

B Finite Simulation-Size Scaling for Thermal Conductivity

For the LJ argon system studied in Section 3.1, a finite simulation-size scaling procedure[24,60] is used to compare the thermal conductivity predictions from Φ and Φ' to those from the Green-Kubo method. The scaling procedure is demonstrated in Fig. 13. The thermal conductivity is predicted from Φ or Φ' and MD simulations with $N_0 = 4, 6, 8$, and 10. The bulk conductivity, k_∞, is then estimated by fitting the data to

$$1/k = 1/k_\infty + A/N_0, \tag{30}$$

where A is a constant. This procedure is necessary because the first Brillouin zone is only sampled at a finite number of points for a finite simulation size, with no contribution from the volume at its center. To predict a bulk thermal conductivity, it is important to sample points near the Brillouin zone center, where the modes can have large lifetimes and group velocities.[50,60]

C Derivation of Phonon Spectral Energy Density

To derive the phonon Spectral Energy Density, Φ, we begin with harmonic lattice dynamics theory.[14,63] In reciprocal space, the system Hamiltonian, H, is

$$\begin{aligned} H =& \frac{1}{2}\sum_{\boldsymbol{\kappa},\nu}^{N,3n}\left[\dot{q}^*(\tbinom{\boldsymbol{\kappa}}{\nu};t)\,\dot{q}(\tbinom{\boldsymbol{\kappa}}{\nu};t)+\omega_0^2(\tbinom{\boldsymbol{\kappa}}{\nu})\,q^*(\tbinom{\boldsymbol{\kappa}}{\nu};t)\,q(\tbinom{\boldsymbol{\kappa}}{\nu};t)\right] \\ =& \sum_{\boldsymbol{\kappa},\nu}^{N,3n}\left[T(\tbinom{\boldsymbol{\kappa}}{\nu};t)+V(\tbinom{\boldsymbol{\kappa}}{\nu};t)\right], \end{aligned} \tag{31}$$

where t is time, $\omega_0(\tbinom{\boldsymbol{\kappa}}{\nu})$ is the frequency of the phonon mode denoted by wave vector $\boldsymbol{\kappa}$ and dispersion branch ν, and N and n are the total number of unit cells and the number of atoms in the unit cell. The Hamiltonian is the total system energy and is the sum of the mode- and time-dependent kinetic and potential energies, $T(\tbinom{\boldsymbol{\kappa}}{\nu};t)$ and $V(\tbinom{\boldsymbol{\kappa}}{\nu};t)$. The phonon normal mode coordinate, $q(\tbinom{\boldsymbol{\kappa}}{\nu};t)$ and its time derivative, $q(\tbinom{\boldsymbol{\kappa}}{\nu};t)$, are given by

$$q(\tbinom{\boldsymbol{\kappa}}{\nu};t) = \sum_{\alpha,b,l}^{3,n,N}\sqrt{\frac{m_b}{N}}u_\alpha(\tbinom{l}{b};t)\,e^*(\tbinom{\boldsymbol{\kappa}\ b}{\nu\ \alpha})\exp[i\boldsymbol{\kappa}\cdot\mathbf{r}_0(\tbinom{l}{0})] \tag{32}$$

and

$$\dot{q}(\tbinom{\boldsymbol{\kappa}}{\nu};t) = \sum_{\alpha,b,l}^{3,n,N}\sqrt{\frac{m_b}{N}}\dot{u}_\alpha(\tbinom{l}{b};t)\,e^*(\tbinom{\boldsymbol{\kappa}\ b}{\nu\ \alpha})\exp[i\boldsymbol{\kappa}\cdot\mathbf{r}_0(\tbinom{l}{0})], \tag{33}$$

where m_b is the mass of the b^{th} atom in the unit cell and $\mathbf{r}_0(\tbinom{l}{0})$ is the equilibrium position vector of the l^{th} unit cell. The α-component of the displacement from equilibrium, $u_\alpha(\tbinom{l}{b};t)$, and velocity, $\dot{u}_\alpha(\tbinom{l}{b};t)$, of the b^{th} atom in the l^{th} unit cell are time-dependent and are related to the phonon mode coordinates through the time-independent eigenvector that has components $e(\tbinom{\boldsymbol{\kappa}\ b}{\nu\ \alpha})$. We start from Eq. (33) and follow the formulation of anharmonic lattice dynamics theory.[14,33,54,63] In an anharmonic system, the phonon populations fluctuate about the equilibrium distribution function.[63] The phonon mode coordinate for the mode described by $(\boldsymbol{\kappa},\nu)$ and its time derivative can be written as

$$q(\tbinom{\boldsymbol{\kappa}}{\nu};t) = q_{SS}(\tbinom{\boldsymbol{\kappa}}{\nu};t) + q_T(\tbinom{\boldsymbol{\kappa}}{\nu};t) \tag{34}$$

and

$$\dot{q}(\tbinom{\boldsymbol{\kappa}}{\nu};t) = \dot{q}_{SS}(\tbinom{\boldsymbol{\kappa}}{\nu};t) + \dot{q}_T(\tbinom{\boldsymbol{\kappa}}{\nu};t)\,. \tag{35}$$

The steady-state (SS) and transient (T) parts and their time derivatives are given by

$$\begin{aligned} q_{SS}(\tbinom{\boldsymbol{\kappa}}{\nu};t) =& C_1(\tbinom{\boldsymbol{\kappa}}{\nu})\exp[i\omega_0(\tbinom{\boldsymbol{\kappa}}{\nu})\,t] \\ &+ C_2(\tbinom{\boldsymbol{\kappa}}{\nu})\exp[-i\omega_0(\tbinom{\boldsymbol{\kappa}}{\nu})\,t], \end{aligned} \tag{36}$$

$$\begin{aligned} q_T(\boldsymbol{\kappa}_\nu;t) =& \exp[-\Gamma(\boldsymbol{\kappa}_\nu)\,|t|]\{C_3(\boldsymbol{\kappa}_\nu)\exp[i\omega_0(\boldsymbol{\kappa}_\nu)\,t] \\ & - C_4(\boldsymbol{\kappa}_\nu)\exp[-i\omega_0(\boldsymbol{\kappa}_\nu)\,t]\}, \end{aligned} \tag{37}$$

$$\dot{q}_{SS}(\boldsymbol{\kappa}_\nu;t) = i\omega_0\left\{C_1(\boldsymbol{\kappa}_\nu)\exp[i\omega_0(\boldsymbol{\kappa}_\nu)\,t] - C_2(\boldsymbol{\kappa}_\nu)\exp[-i\omega_0(\boldsymbol{\kappa}_\nu)\,t]\right\}, \tag{38}$$

and

$$\begin{aligned} \dot{q}_T(\boldsymbol{\kappa}_\nu;t) =& \exp[-\Gamma(\boldsymbol{\kappa}_\nu)\,|t|]\{C_3(\boldsymbol{\kappa}_\nu)\,[i\omega_0(\boldsymbol{\kappa}_\nu) - \Gamma(\boldsymbol{\kappa}_\nu)]\exp[i\omega_0(\boldsymbol{\kappa}_\nu)\,t] \\ & -C_4(\boldsymbol{\kappa}_\nu)\,[i\omega_0(\boldsymbol{\kappa}_\nu) + \Gamma(\boldsymbol{\kappa}_\nu)]\exp[-i\omega_0(\boldsymbol{\kappa}_\nu)\,t]\,\}, \end{aligned} \tag{39}$$

where the Cs are constants and $\omega_0(\boldsymbol{\kappa}_\nu)$ and $\Gamma(\boldsymbol{\kappa}_\nu)$ are the phonon mode frequency and linewidth. The transient part describes the creation of an excess in the population of a phonon mode for $t < 0$ and its decay back to equilibrium for $t > 0$. Phonon population fluctuations are commonly modeled using the excitation and decay of a single phonon mode (i.e., the single mode relaxation time approximation). In a real system, there will be multiple phonons in each mode that simultaneously grow or decay with time. Thus, dealing only with $\dot{q}$, we let

$$\begin{aligned} \dot{q}(\boldsymbol{\kappa}_\nu;t) =& \sum_j i\exp[-\Gamma(\boldsymbol{\kappa}_\nu)\,|t-t_j|]\times \\ & \{A_j(\boldsymbol{\kappa}_\nu)\,[\omega_0(\boldsymbol{\kappa}_\nu) + i\Gamma(\boldsymbol{\kappa}_\nu)]\exp[i\omega_0(\boldsymbol{\kappa}_\nu)\,(t-t_j)] \\ & - B_j(\boldsymbol{\kappa}_\nu)\,[\omega_0(\boldsymbol{\kappa}_\nu) - i\Gamma(\boldsymbol{\kappa}_\nu)]\exp[-i\omega_0(\boldsymbol{\kappa}_\nu)\,(t-t_j)]\,\}, \end{aligned} \tag{40}$$

where many phonons in each mode, indexed by j, are simultaneously being created and destroyed. The phonons grow for $t < t_j$, decay for $t > t_j$, and A_j and B_j are constants. We are not concerned with the values of t_j, A_j, and B_j, though they should satisfy the long-time average $\langle \dot{q}^*(\boldsymbol{\kappa}_\nu;t)\,\dot{q}(\boldsymbol{\kappa}_\nu;t)\rangle = \langle \dot{q}^*_{SS}(\boldsymbol{\kappa}_\nu;t)\,\dot{q}_{SS}(\boldsymbol{\kappa}_\nu;t)\rangle$. The expectation value of the kinetic energy of the normal mode in the time domain is

$$\langle T(\boldsymbol{\kappa}_\nu)\rangle = \frac{1}{2}\lim_{\tau_0\to\infty}\frac{1}{\tau_0}\int_0^{\tau_0}\dot{q}^*(\boldsymbol{\kappa}_\nu;t)\,\dot{q}(\boldsymbol{\kappa}_\nu;t)\,dt. \tag{41}$$

The expectation value of the kinetic energy of the normal mode can be transformed from the time domain to the frequency domain by Parseval's theorem,[48] giving

$$T(\boldsymbol{\kappa}_\nu;\omega) = \lim_{\tau_0\to\infty}\frac{1}{2\tau_0}\left|\frac{1}{\sqrt{2\pi}}\int_0^{\tau_0}\dot{q}(\boldsymbol{\kappa}_\nu;t)\exp(-i\omega t)dt\right|^2. \tag{42}$$

By substituting Eq. (40) into Eq. (42) and performing the time integration we find

$$\begin{aligned} T(\boldsymbol{\kappa}_\nu;\omega) = \frac{1}{16\pi\tau_0}\Bigg|\sum_j \exp[-i\omega t_j]\Bigg\{ & A_j(\boldsymbol{\kappa}_\nu)\,\frac{\omega_0(\boldsymbol{\kappa}_\nu) + i\Gamma(\boldsymbol{\kappa}_\nu)}{\omega_0(\boldsymbol{\kappa}_\nu) - \omega + i\Gamma(\boldsymbol{\kappa}_\nu)} \\ & + B_j(\boldsymbol{\kappa}_\nu)\,\frac{\omega_0(\boldsymbol{\kappa}_\nu) - i\Gamma(\boldsymbol{\kappa}_\nu)}{\omega_0(\boldsymbol{\kappa}_\nu) + \omega - i\Gamma(\boldsymbol{\kappa}_\nu)}\Bigg\}\Bigg|^2. \end{aligned} \tag{43}$$

We are primarily interested in values of ω where $\omega \approx \omega_0$ when $\Gamma << \omega_0$ (this condition is met for the three systems studied here). When $\omega \approx \omega_0$, the term involving A_j becomes large and the term involving B_j can be neglected (alternatively, we could ignore the term involving A_j when $\omega \approx -\omega_0$). Hence, we find

$$\begin{aligned} T(\boldsymbol{\kappa}_\nu;\omega) = \frac{1}{16\pi\tau_0}\sum_j\sum_{j'}\cos\left[\omega(t_{j'}-t_j)\right]A_j(\boldsymbol{\kappa}_\nu)\,A_{j'}(\boldsymbol{\kappa}_\nu) \\ \times\frac{\omega_0^2(\boldsymbol{\kappa}_\nu)+\Gamma^2(\boldsymbol{\kappa}_\nu)}{\Gamma(\boldsymbol{\kappa}_\nu)}\frac{\Gamma(\boldsymbol{\kappa}_\nu)}{[\omega_0(\boldsymbol{\kappa}_\nu)-\omega]^2+\Gamma^2(\boldsymbol{\kappa}_\nu)}. \end{aligned} \tag{44}$$

We arrive at the expression for the phonon spectral energy density for the wavevector $\boldsymbol{\kappa}$ by summing Eq. (44) over the different polarizations ν,

$$\Phi(\boldsymbol{\kappa},\omega) = 2\sum_\nu^{3n} T(\boldsymbol{\kappa}_\nu;\omega) = \sum_\nu^{3n} C_0(\boldsymbol{\kappa}_\nu)\,\frac{\Gamma(\boldsymbol{\kappa}_\nu)/\pi}{[\omega_0(\boldsymbol{\kappa}_\nu)-\omega]^2+\Gamma^2(\boldsymbol{\kappa}_\nu)}, \tag{45}$$

where the factor of two comes from equipartition of kinetic and potential energy (valid for a harmonic classical system), and

$$C_0(\boldsymbol{\kappa}_\nu) = \sum_j\sum_{j'}\cos\left[\omega(t_{j'}-t_j)\right]A_j(\boldsymbol{\kappa}_\nu)\,A_{j'}(\boldsymbol{\kappa}_\nu)\,\frac{\omega_0^2(\boldsymbol{\kappa}_\nu)+\Gamma^2(\boldsymbol{\kappa}_\nu)}{8\tau_0\Gamma(\boldsymbol{\kappa}_\nu)}. \tag{46}$$

Thus, the phonon spectral energy density $\Phi(\boldsymbol{\kappa},\omega)$ is a superposition of $3n$ Lorentzian functions with centers at $\omega_0(\boldsymbol{\kappa}_\nu)$ (one for each polarization) with a linewidth (half-width at half-maximum) of $\Gamma(\boldsymbol{\kappa}_\nu)$. Φ is a spectral energy density since its integral over all wavevectors and frequencies is the total crystal energy, i.e., the Hamiltonian is

$$H = \int_{V_{BZ}}\int_0^\infty \Phi(\boldsymbol{\kappa},\omega)d\omega d\boldsymbol{\kappa}, \tag{47}$$

where V_{BZ} is the volume of the first Brillouin zone. Like the frequency broadening, there is also a broadening of the SED in wavevector.[59] For a finite sampling of the first Brillouin zone, the Hamiltonian can be approximated by

$$H \approx 2\sum_{\boldsymbol{\kappa},\nu}^{N,3n}\langle T(\boldsymbol{\kappa}_\nu;t)\rangle = \sum_{\boldsymbol{\kappa}}^{N}\int_0^\infty \Phi(\omega,\boldsymbol{\kappa})d\omega. \tag{48}$$

References

[1] Philip B. Allen and Joseph L. Feldman. Thermal conductivity of disordered harmonic solids. *Physical Review B*, 48(17):12581–12588, Nov 1993.

[2] N. W. Ashcroft and N. D. Mermin. *Solid State Physics*. Saunders, Fort Worth, 1976.

[3] S. Baroni, S. de Gironcoli, A. Dal Corso, and P. Giannozzi. Phonons and related crystal properties from density-functional perturbation theory. *Reviews of Modern Physics*, 73:515–562, 2001.

[4] N. Bernstein, J. L. Feldman, and D. J. Singh. Calculations of dynamical properties of skutterudites: Thermal conductivity, thermal expansivity, and atomic mean-square displacement. *Phys. Rev. B*, 81:134301, Apr 2010.

[5] D. G. Cahill, S. K. Watson, and R. O. Pohl. Lower limit to thermal conductivity of disordered crystals. *Physical Review B*, 46:6131–6140, 1992.

[6] David G. Cahill and R. O. Pohl. Thermal conductivity of amorphous solids above the plateau. *Physical Review B*, 35:40674073, 1987.

[7] David G. Cahill, Fumiya Watanabe, Angus Rockett, and Cronin B. Vining. Thermal conductivity of epitaxial layers of dilute sige alloys. *Phys. Rev. B*, 71:235202, Jun 2005.

[8] David G. Cahill, S. K. Watson, and R. O. Pohl. Lower limit to the thermal conductivity of disordered crystals. *Phys. Rev. B*, 46:6131–6140, Sep 1992.

[9] J. Callaway. Model for lattice thermal conductivity at low temperatures. *Physical Review*, 113:1046, 1959.

[10] G Chen, M S Dresselhaus, G Dresselhaus, J Fleurial, and T Caillat. Recent developments in thermoelectric materials. *International Materials Reviews*, 48(1):45–66, 2003.

[11] Mogens Christensen, Nina Lock, Jacob Overgaard, and Bo B. Iversen. Crystal structures of thermoelectric n- and p-type ba8ga16ge30 studied by single crystal, multitemperature, neutron diffraction, conventional x-ray diffraction and resonant synchrotron x-ray diffraction. *Journal of the American Chemical Society*, 128(49):15657–15665, 2006.

[12] J. L. Cohn, G. S. Nolas, V. Fessatidis, T. H. Metcalf, and G. A. Slack. Glasslike heat conduction in high-mobility crystalline semiconductors. *Phys. Rev. Lett.*, 82:779–782, Jan 1999.

[13] R. M. Costescu, D. G. Cahill, F. H. Fabreguette, Z. A. Sechrist, and S. M. George. Ultra-low thermal conductivity in W/Al_2O_3 nanolaminates. *Science*, 303:989–990, 2004.

[14] M. T. Dove. *Introduction to Lattice Dynamics*. Cambridge, Cambridge, 1993.

[15] M.S. Dresselhaus, G. Chen, M.Y. Tang, R.G. Yang, H. Lee, D.Z. Wang, Z.F. Ren, J.P. Fleurial, and P. Gogna. New directions for low-dimensional thermoelectric materials. *Advanced Materials*, 19(8):1043–1053, 2007.

[16] A. Dyer. *An Introduction to Zeolite Molecular Sieves*. Wiley, Chichester, 1988.

[17] Mohamed Eddaoudi, David B. Moler, Hailian Li, Banglin Chen, Theresa M. Reineke, Michael O'Keeffe, and Omar M. Yaghi. Modular chemistry: Secondary building units as a basis for the design of highly porous and robust metal-organic carboxylate frameworks. *Accounts of Chemical Research*, 34(4):319–330, 2001. PMID: 11308306.

[18] A. Einstein. Elementare betrachtungen uber die thermische molekularbewegung in festen korper. *Annalen der Physik*, 35:679–694, 2010.

[19] J. J. Freeman and A. C. Anderson. Thermal conductivity of amorphous solids. *Physical Review B*, 34:56845690, 1986.

[20] J. V. Goicochea, M. Madrid, and C. H. Amon. Thermal properties for bulk silicon based on the determination of relaxation times using molecular dynamics. *Journal of Heat Transfer*, 132:012401, 2010.

[21] J. E. Graebner, B. Golding, and L. C. Allen. Phonon localization in glasses. *Phys. Rev. B*, 34:5696–5701, Oct 1986.

[22] T.M. Tritt G.S. Nolas, D.T. Morelli. Skutterudites: A phonon-glass-electron crystal approach to advanced thermoelectric energy conversion applications. *Annu. Rev. Mater. Sci.*, 29:86–116, 1999.

[23] Tao He, Jiazhong Chen, H. David Rosenfeld, and M. A. Subramanian. Thermoelectric properties of indium-filled skutterudites. *Chemistry of Materials*, 18(3):759–762, 2006.

[24] Yuping He, Davide Donadio, and Giulia Galli. Heat transport in amorphous silicon: Interplay between morphologyand disorder. *Applied Physics Letters*, 98:144101, 2011.

[25] M. G. Holland. Analysis of lattice thermal conductivity. *Physical Review*, 132:2461, 1963.

[26] C. H. Amon A. J. H. McGaughey J. M. Larkin J. E. Turney, A. D. Massicotte. Comparison and evaluation of spectral energy methods for predicting phonon properties. *in submission*, 2012.

[27] V. Keppens, D. Mandrus, B. C. Sales, B. C. Chakoumakos, P. Dai, R. Coldea, M. B. Maple, D. A. Gajewski, E. J. Freeman, and S. Bennington. Localized vibrational modes in metallic solids. *Nature*, 395(876), 1998.

[28] C. Kittel. Interpretation of the thermal conductivity of glasses. *Physical Review*, 75:974, 1949.

[29] P G Klemens. The scattering of low-frequency lattice waves by static imperfections. *Proceedings of the Physical Society. Section A*, 68(1113), 1955.

[30] P G Klemens. Thermal resistance due to isotopic mass variation. *Proceedings of the Physical Society. Section A*, 70(11):833, 1957.

[31] A. J. C. Ladd, B. Moran, and W. G. Hoover. Lattice thermal conductivity: A comparison of molecular dynamics and anharmonic lattice dynamics. *Physical Review B*, 34:5058–5064, 1986.

[32] Xiao Liu, J. L. Feldman, D. G. Cahill, R. S. Crandall, N. Bernstein, D. M. Photiadis, M. J. Mehl, and D. A. Papaconstantopoulos. High thermal conductivity of a hydrogenated amorphous silicon film. *Phys. Rev. Lett.*, 102:035901, Jan 2009.

[33] A. A. Maradudin. In G. K. Horton and A. A. Maradudin, editors, *Dynamical Properties of Solids, Volume 1*, pages 1–82. Elsevier, New York, 1974.

[34] A. A. Maradudin and A. E. Fein. Scattering of neutrons by an anharmonic crystal. *Physical Review*, 128:2589–2608, 1962.

[35] A. J. H. McGaughey, M. I. Hussein, E. S. Landry, M. Kaviany, and G. M. Hulbert. Phonon band structure and thermal transport correlation in a layered diatomic crystal. *Physical Review B*, 74:104304, 2006.

[36] A. J. H. McGaughey and M. Kaviany. Quantitative validation of the Boltzmann transport equation phonon thermal conductivity model under the single-mode relaxation time approximation. *Physical Review B*, 69:094303, 2004.

[37] A. J. H. McGaughey and M. Kaviany. Thermal conductivity decomposition and analysis using molecular dynamics simulations. Part I. Lennard-Jones argon. *International Journal of Heat and Mass Transfer*, 47:1783–1798, 2004.

[38] A. J. H. McGaughey and M. Kaviany. Thermal conductivity decomposition and analysis using molecular dynamics simulations. Part II. Complex silica structures. *International Journal of Heat and Mass Transfer*, 47:1799–1816, 2004.

[39] Alan J. H. McGaughey and Ankit Jain. Nanostructure thermal conductivity prediction by monte carlo sampling of phonon free paths. *Applied Physics Letters*, 100(6):061911, 2012.

[40] D. A. McQuarrie. *Statistical Mechanics*. University Science Books, Sausalito, 2000.

[41] A. J. Minnich, M. S. Dresselhaus, Z. F. Ren, and G. Chen. Bulk nanostructured thermoelectric materials: current research and future prospects. *Energy Environ. Sci.*, 2:–, 2009.

[42] A. Miyamoto and M. Kubo. Structure and dynamics of ion-exchanged zeolites as investigated by molecular dynamics and computer graphics. 83:117 – 124, 1994.

[43] Niels B. Christensen Fanni Juranyi Niels H. Andersen Kim Lefmann Jakob Andreasson Christian R. H. Bahl Mogens Christensen, Asger B. Abrahamsen and Bo B. Iversen. Avoided crossing of rattler modes in thermoelectric materials. *Nature Materials*, 7:811–815, 2008.

[44] S Moon. Thermal conductivity of amorphous silicon thin films. *International Journal of Heat and Mass Transfer*, 45(12):2439–2447, 2002.

[45] M. O'Keeffe, M. Eddaoudi, Hailian Li, T. Reineke, and O.M. Yaghi. Frameworks for extended solids: Geometrical design principles. *Journal of Solid State Chemistry*, 152(1):3 – 20, 2000.

[46] Zhun-Yong Ong, Eric Pop, and Junichiro Shiomi. Reduction of phonon lifetimes and thermal conductivity of a carbon nanotube on amorphous silica. *Physical Review B*, 84(16):165418, 2011.

[47] P. F. Qiu, J. Yang, R. H. Liu, X. Shi, X. Y. Huang, G. J. Snyder, W. Zhang, and L. D. Chen. High-temperature electrical and thermal transport properties of fully filled skutterudites rfe[sub 4]sb[sub 12] (r = ca, sr, ba, la, ce, pr, nd, eu, and yb). *Journal of Applied Physics*, 109(6):063713, 2011.

[48] W. Rudin. *Real and Complex Analysis*. McGraw-Hill, New York, 1987.

[49] Brian C Sales, B C Chakoumakos, David Mandrus, and J W Sharp. Atomic displacement parameters and the lattice thermal conductivity of clathrate-like thermoelectric compounds. *Journal of Solid State Chemistry*, 146(2):528–532, 1999.

[50] D. P. Sellan, J. E. Turney, A. J. H. McGaughey, and C. H. Amon. Cross-plane phonon transport in thin films. *Journal of Applied Physics*, 108:113524, 2010.

[51] Sergei Shenogin, Arun Bodapati, Pawel Keblinski, and Alan J. H. McGaughey. Predicting the thermal conductivity of inorganic and polymeric glasses: The role of anharmonicity. *Journal of Applied Physics*, 105(3):034906, 2009.

[52] Junichiro Shiomi, Keivan Esfarjani, and Gang Chen. Thermal conductivity of half-heusler compounds from first-principles calculations. *Physical Review B*, 84(10):125209, 2011.

[53] G. A. Slack. Solid state physics. *Solid State Physics*, 34:15657–15665, 1979.

[54] G. P. Srivastava. *The Physics of Phonons*. Adam Hilger, Bristol, 1990.

[55] E. F. Steigmeier and I. Kudman. Acoustical-optical phonon scattering in ge, si, and iii-v compounds. *Phys. Rev.*, 141:767–774, Jan 1966.

[56] R. B. Stephens. Low-temperature specific heat and thermal conductivity of noncrystalline dielectric solids. *Physical Review B*, 8:28962905, 1973.

[57] J. A. Thomas, J. E. Turney, R. M. Iutzi, C. H. Amon, and A. J. H. McGaughey. Predicting phonon dispersion relations and lifetimes from the spectral energy density. *Physical Review B*, 81:081411(R), 2010.

[58] Eric S. Toberer, Alex Zevalkink, and G. Jeffrey Snyder. Phonon engineering through crystal chemistry. *J. Mater. Chem.*, 21, 2011.

[59] J. E. Turney. *Predicting phonon properties and thermal conductivity using anharmonic lattice dynamics calculations*. PhD Thesis, Carnegie Mellon University, Pittsburgh, PA, 2009.

[60] J. E. Turney, E. S. Landry, A. J. H. McGaughey, and C. H. Amon. Predicting phonon properties and thermal conductivity from anharmonic lattice dynamics calculations and molecular dynamics simulations. *Physical Review B*, 79:064301, 2009.

[61] J. E. Turney, A. J. H. McGaughey, and C. H. Amon. Thin film thermal conductivity by anharmonic lattice dynamics calculations. In *Proceedings of IMECE 2008*. ASME, 2008. Paper number IMECE2008-66697.

[62] Vincenzo Vitelli, Ning Xu, Matthieu Wyart, Andrea J. Liu, and Sidney R. Nagel. Heat transport in model jammed solids. *Phys. Rev. E*, 81:021301, Feb 2010.

[63] D. C. Wallace. *Thermodynamics of Crystals*. Cambridge Univ. Press, Cambridge, UK, 1972.

[64] Xiao-Jun Wang, Mei-Bo Tang, Jing-Tai Zhao, Hao-Hong Chen, and Xin-Xin Yang. Thermoelectric properties and electronic structure of zintl compound bazn[sub 2]sb[sub 2]. *Applied Physics Letters*, 90(23):232107, 2007.

[65] et al. Yang. Effect of la filling on thermoelectric properties of laxco36ni04sb12-filled skutterudite prepared by ma-hp method. *Jo. of Sol. Stat. Chem.*, 179:212–216, 2006.

[66] Ho-Soon Yang, David G. Cahill, X. Liu, J. L. Feldman, R. S. Crandall, B. A. Sperling, and J. R. Abelson. Anomalously high thermal conductivity of amorphous si deposited by hot-wire chemical vapor deposition. *Phys. Rev. B*, 81:104203, Mar 2010.

[67] Mona Zebarjadi, Keivan Esfarjani, Jian Yang, Z. F. Ren, and Gang Chen. Effect of filler mass and binding on thermal conductivity of fully filled skutterudites. *Phys. Rev. B*, 82:195207, Nov 2010.

[68] J. M. Ziman. *Electrons and Phonons*. Oxford, New York, 2001.

[69] B L Zink, R Pietri, and F Hellman. Thermal conductivity and specific heat of thin-film amorphous silicon. *Physical Review Letters*, 96(5):055902, 2006.